

Analytical Galaxy Profiles for Photometric and Lensing Analysis

David N. Spergel

Department of Astrophysical Sciences, Princeton University,

Princeton NJ 08544 USA

Institute of Physics and Mathematics of the Universe (IPMU),

Kashiwa, Japan

November 21, 2018

Received _____; accepted _____

ABSTRACT

This article introduces a family of analytical functions of the form $x^\nu K_\nu(x)$, where K_ν is the incomplete Bessel function of the third kind. This family of functions can describe the density profile, projected and integrated light profiles and the gravitational potentials of galaxies. For the proper choice of parameters, these functions accurately approximate Sersic functions over a range of indices and are good fits to galaxy light profiles. With an additional parameter corresponding to a galaxy core radius, these functions can fit galaxy like M87 over a factor of 10^5 in radius. Unlike Sersic profiles, these functions have simple analytical 2-dimensional and 3-dimensional Fourier transforms, so they are easily convolved with spatially varying point spread function and are well suited for photometric and lensing analysis. We use these functions to estimate the effects of seeing on lensing measurements and show that high S/N measurements, even when the PSF is larger than the galaxy effective radius, should be able to recover accurate estimates of lensing distortions by weighting light in the outer isophotes that are less effected by seeing.

1. Introduction

Weak lensing observations have the potential to provide powerful new insights into the nature of dark energy and dark matter (see e.g., (Hoekstra & Jain 2008)) as well as directly the relationship between luminous and dark matter.

Over the next few years, astronomers can anticipate very large, high quality photometric data. It is essential to develop image analysis techniques that can exploit this high quality data. The analysis techniques must be rapid and unbiased. Ideally, they should be nearly

optimal and use most of the information in an astronomical image. While there has been significant progress in the past few years, astronomers have not yet converged on an approach for image analysis (Bridle et al. 2009).

Most image analysis takes one of two approaches: (1) fit an analytical form to the light profile such as the Sersic profile to the galaxy distribution or (2) use an orthogonal basis function to characterize the ellipticity of an image. While Sersic profiles have proven to be remarkably successful at fitting galaxy light profiles outside of the central cores of galaxies (Kormendy et al. (2009)), applying them to galaxy images requires non-linear fits to the data (Ngan et al. 2009) and computing the effects of seeing is computationally demanding. The later approach (e.g., (Bernstein & Jarvis 2002)) is computationally simpler and mathematically elegant; however, Gaussians are poor approximations to galaxies.

The goal of this paper is to define a basis function that combines the advantages of both approaches. §2 introduces a series of functions, $u^\nu K_\nu(u)$ that have a simple representation in Fourier space, so can be easily used in image analysis, and are good approximation to Sersic profiles and more importantly to galaxy photometry. §3 generalizes these functions to triaxial systems. §4 applies these functions for galaxy photometry and §5 considers the effects of seeing and its implications for lensing measurements.

2. Analytical Functions for Starlight Profiles

We consider a family of models whose 3-d Fourier profile has the form:

$$\rho_\nu(k) = \frac{L_0}{4\pi^2 \left[1 + (k_x^2 + k_y^2 + k_z^2) \left(\frac{r_0}{c_\nu} \right)^2 \right]^{1+\nu}} \quad (1)$$

where r_0 is the half-light radius, c_ν is a constant given in table 1 and $\nu > -1$. Projecting this to two dimensions, the Fourier transform retains its simple form:

$$\Sigma_\nu(k) = \frac{L_0}{2\pi \left[1 + (k_x^2 + k_y^2) \left(\frac{r_0}{c_\nu} \right)^2 \right]^{1+\nu}} \quad (2)$$

Moving to real space, these profiles correspond to analytical 2-dimensional profiles:

$$\begin{aligned} \Sigma_\nu(r) &= \int k dk J_0(kr) \frac{L_0}{\left[1 + k^2 \left(\frac{r_0}{c_\nu} \right)^2 \right]^{1+\nu}} \\ &= \frac{c_\nu^2 L_0}{r_0^2} f_\nu \left(\frac{c_\nu r}{r_0} \right) \end{aligned} \quad (3)$$

where

$$f_\nu(u) = \left(\frac{u}{2} \right)^\nu \frac{K_\nu(u)}{\Gamma(\nu + 1)}, \quad (4)$$

and $K_\nu(u)$ is a modified spherical Bessel function of the third kind. The Appendix describes some useful properties of these functions.

For $\nu = j + 1/2$, this has a simple form:

$$f_{-1/2}(u) = \frac{\exp(-u)}{u} \quad (5)$$

$$f_{1/2}(u) = \exp(-u) \quad (6)$$

$$f_{3/2}(u) = \frac{1}{3} \exp(-u) (u + 1) \quad (7)$$

At small u , $f_\nu(u) \rightarrow 1/(2(\nu + 1))$ for $\nu \geq 0$ and $f_\nu(u) \rightarrow u^{2\nu}/(2(\nu + 1))$ for $-1 < \nu < 0$. At large u , $f_\nu(u) \rightarrow \sqrt{\pi/2} \exp(-u) u^{-1/2+\nu}$.

By going back to Fourier space and integrating by parts, we can analytically evaluate

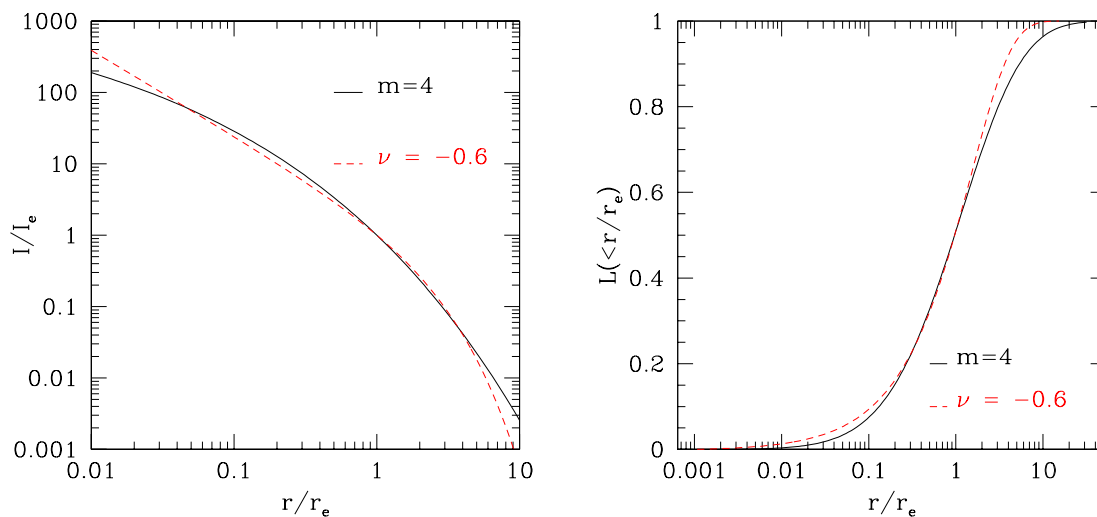


Fig. 1.— This pair of figures shows that a $\nu = -0.6$ density profile and a deVaucouleur’s law profile ($m = 4$ Sersic profile) have similar forms. The left panel compares the surface density profile for the two models. The right panel compares the integrated surface density profiles (Equation (8)).

the integrated light profile of the one component model,

$$\begin{aligned}
 L(r') &= 2\pi \int_0^{r'} \Sigma(R) R dR \\
 &= L_0 \int_0^{r'} R dR \int_0^\infty k dk \frac{J_0(kR)}{\left[1 + k^2 \left(\frac{r_0}{c_\nu}\right)^2\right]^{1+\nu}} \\
 &= L_0 r' \int_0^\infty dk \frac{J_1(kr')}{\left[1 + k^2 \left(\frac{r_0}{c_\nu}\right)^2\right]^{1+\nu}} \\
 &= L_0 \left\{ 1 - \frac{2(1+\nu)r_0^2}{c_\nu^2} \int_0^\infty \frac{k dk J_0(kr')}{\left[1 + k^2 \left(\frac{r_0}{c_\nu}\right)^2\right]^{2+\nu}} \right\} \\
 &= L_0 \left[1 - 2(1+\nu) f_{\nu+1} \left(\frac{c_\nu r'}{r_0} \right) \right] \tag{8}
 \end{aligned}$$

Using equation (8), we can solve $(1 + \nu)f_{\nu+1}(c_\nu) = 1/4$ and determine the half-light radius for the distribution. Table 1 lists the values of the c_ν so that r_0 is the half-light radius for the light distribution.

We can also evaluate the 3-dimensional density profile,

$$\begin{aligned}
 \rho_\nu(r) &= \int_0^\infty k^2 dk j_0(kr) \frac{L_0}{\pi \left[1 + k^2 \left(\frac{r_0}{c_\nu}\right)^2\right]^{1+\nu}} \\
 &= \frac{L_0 c_\nu^3}{r_0^3} \frac{\pi^{1/2} \Gamma(\nu + \frac{1}{2})}{2\Gamma(\nu + 1)} f_{\nu-\frac{1}{2}} \left(\frac{c_\nu r}{r_0} \right). \tag{9}
 \end{aligned}$$

We can evaluate the potential,

$$\Phi_\nu(r) = -2GM \int_0^\infty dk \frac{j_0(kr) dk}{\pi \left[1 + k^2 \left(\frac{r_0}{c_\nu}\right)^2\right]^{1+\nu}} \tag{10}$$

Table 1: Half-light Radii

ν	c_ν	ν	c_ν	ν	c_ν	ν	c_ν
-0.90	0.03502	-0.45	0.76039	0.00	1.25715	0.45	1.64014
-0.85	0.11212	-0.40	0.82451	0.05	1.30390	0.50	1.67835
-0.80	0.20379	-0.35	0.88584	0.10	1.34943	0.55	1.71585
-0.75	0.29616	-0.30	0.94468	0.15	1.39383	0.60	1.75270
-0.70	0.38480	-0.25	1.00128	0.20	1.43717	0.65	1.78891
-0.65	0.46864	-0.20	1.05585	0.25	1.47952	0.70	1.82453
-0.60	0.54771	-0.15	1.10856	0.30	1.52093	0.75	1.85957
-0.55	0.62240	-0.10	1.15960	0.35	1.56148	0.80	1.89406
-0.50	0.69315	-0.05	1.20909	0.40	1.60120	0.85	1.92803

by first multiplying by r and differentiating,

$$\begin{aligned}
 \frac{\partial}{\partial r}(r\Phi_\nu(r)) &= -2GM \int_0^\infty \frac{\cos(kr)dk}{\pi \left[1 + k^2 \left(\frac{r_0}{c_\nu}\right)^2\right]^{1+\nu}} \\
 &= -GL_0 \frac{2\Gamma(\nu + 3/2)}{\sqrt{\pi}\Gamma(\nu + 1)} f_{\nu+1/2} \left(\frac{c_\nu r}{r_0}\right)
 \end{aligned} \tag{11}$$

and then integrating again with respect to r to find,

$$\begin{aligned}
 \Phi_\nu(r) &= -GL_0 \left[K_{\nu+1/2} \left(\frac{c_\nu r}{r_0}\right) L_{\nu-1/2} \left(\frac{c_\nu r}{r_0}\right) \right. \\
 &\quad \left. + K_{\nu-1/2} \left(\frac{c_\nu r}{r_0}\right) L_{\nu+1/2} \left(\frac{c_\nu r}{r_0}\right) \right]
 \end{aligned} \tag{12}$$

where L_ν is a modified Struve function.

For $\nu = 0$, this reduces to a simple form::

$$\Phi_0(r) = -\frac{GL_0}{r} [1 - \exp(-c_0 r/r_0)] \tag{13}$$

Since $\nu = 0$ is intermediate between an elliptical galaxy profile ($\nu = -0.6$) and an exponential profile ($\nu = 0.5$), it is a simple potential for a plausible generic stellar model.

We can write the potential in an alternative form by recalling the large x expansion of $K_\nu(x)$:

$$K_\nu(x) = \sqrt{\frac{\pi}{2x}} \exp(-x) \left[1 + \sum_j \frac{\prod_{k=1}^j [4\nu^2 - (2j - k)^2]}{j!(8x)^j} \right] \quad (14)$$

and one of the definitions of the incomplete Gamma functions,

$$\int_a^\infty x^{\nu-j} \exp(-x) dx = \Gamma(\nu - j + 1, a) \quad (15)$$

Thus,

$$\begin{aligned} \Phi(r) = & -\frac{GL_0}{r} \frac{\sqrt{2}}{\Gamma(\nu + 1)} \left[\Gamma\left(\nu + 1, \frac{c_\nu r}{r_0}\right) \right. \\ & \left. + \sum_j \frac{w_j \Gamma\left(\nu - j + 1, \frac{c_\nu r}{r_0}\right)}{8^j j!} \right] \end{aligned} \quad (16)$$

where $\Gamma(\alpha, x)$ is the incomplete Gamma function and $w_j = \prod_{k=1}^j [(2\nu + 1)^2 - (2j - k)^2]$.

There are several interesting extensions to the one component representation:

(1) *Fixed ν models* An alternative to using the index of the functions (ν) as one of the parameters in the galaxy fit is to represent the galaxy light profile as a sum of an exponential term ($\nu = 0.5$) and a very extended profile selected to fit galaxies like M87 ($\nu = 0.85$):

$$\begin{aligned} \Sigma(r/r_0) = & L_1 \exp \left[-1.6783 \left(\frac{r}{r_0} - 1 \right) \right] \\ & + L_2 \left(\frac{r}{r_0} \right)^{-0.85} \frac{K_{0.85}(0.35r/r_0)}{K_{0.85}(0.35)} \end{aligned} \quad (17)$$

where r_0 is fit to the scale length of a given galaxy. The coefficient 0.35 was selected so that the two profiles span the same ranges as the Sersic functions, so that most galaxy profiles can be represented as a sum of the two functions with the same value of r_0 . Figure

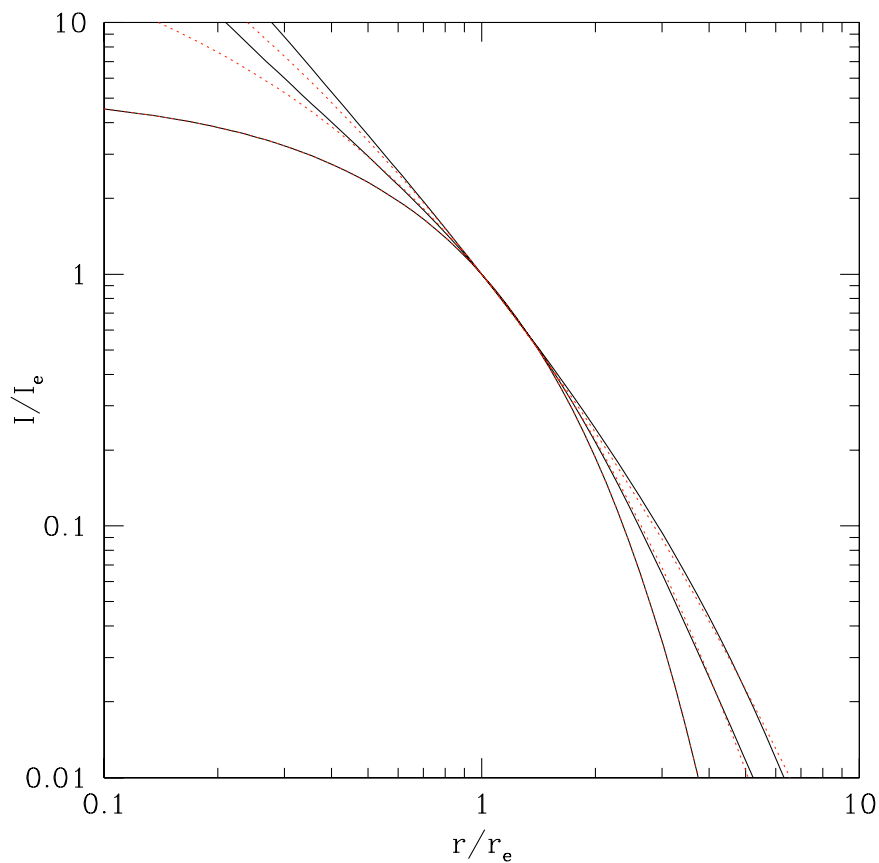


Fig. 2.— This figure compare a linear combination of the modified Bessel function fit (solid lines), $\beta f_{0.5}(c_{0.5}r/r_0) + (1-\beta)f_{-0.85}(0.35r/r_0)$, to the family of Sersic profiles. The solid lines shows the density profiles for $\beta_1 = 0, 0.5$ and 1. The dashed lines show a set of Sersic profiles with $mn = 1, 2$ and 4. The $n = 1$ Sersic profile and the $\beta_1 = 1$ profile are identical.

2 compares Sersic profiles with $m = 1, 2,$ and 4 to surface profiles fit with different linear combinations of the two terms in Equation (17). While the two terms are normalized to have the same amplitude at $r = r_0$, the later term contains more mass for $\beta = 0.5$. Note that this fitting function has three free parameters (L_1, L_2, r_0) , the same number of parameters as the Sersic profile (L, n, r_0) and the profile introduced earlier in this section (L, ν, r_0) . The main advantage of Equation (17) is apparent in §4 where we show that we can precompute the effects of atmospheric seeing.

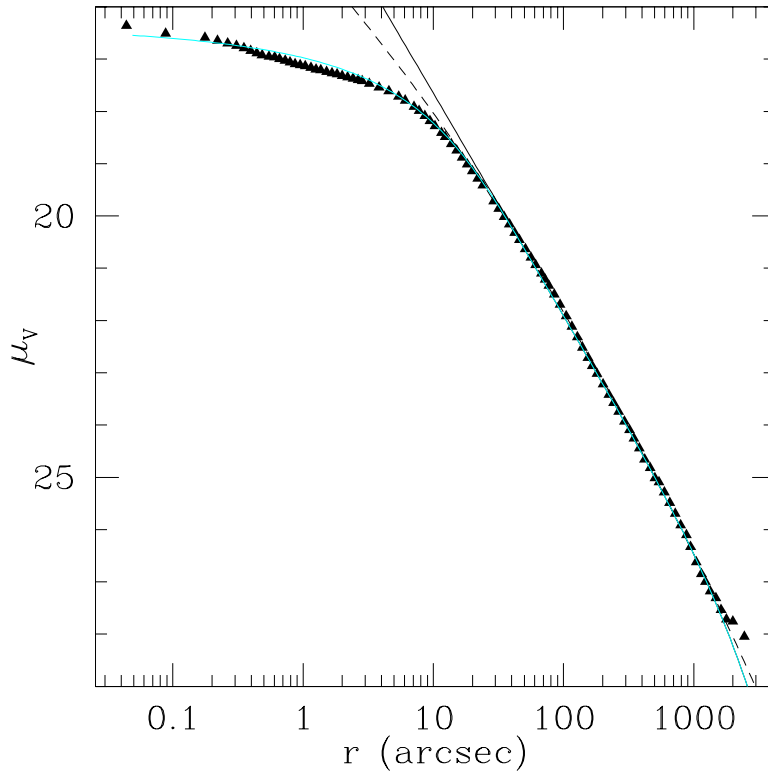


Fig. 3.— This figure compares Kormendy et al. (2009) compilation of observations of M87 (NGC 4468) to their best fit Sersic profile (dashed line with $m = 11.8$ and $r_e = 703.91\text{kpc}$), a one component profile (solid line with $\nu = -0.85$ and $r_0/c_\nu = 1944\text{kpc}$) and a two component profile (cyan solid line with $r_0/c_\nu = 1944\text{kpc}$, $\nu = -0.85$, and $r_{core}/r_0 = 0.0043$).

(2) *Core Radii* For galaxies with well defined cores but extended light profiles (see Figure 3), we can generalize the $\nu < 0$ profile by adding a second component and an additional parameter, r_{core} :

$$\Sigma(r) = \frac{L_0 c_\nu^2}{r_0^2 \left[1 - \left(\frac{r_{core}}{r_0} \right)^{2(1-\nu)} \right]} \left[f_\nu \left(\frac{c_\nu r}{r_0} \right) - \left(\frac{r_{core}}{r_0} \right)^{2\nu} f_\nu \left(\frac{c_\nu r}{r_{core}} \right) \right] \quad (18)$$

This two component form approaches an exponential for $r < r_{core} < r_0$. This generalized surface brightness distribution also has a simple representation in Fourier space:

$$\Sigma(k) = \frac{L_0}{r_0^{2\nu} - r_{core}^{2\nu}} \left[\frac{r_0^{2\nu}}{(1 + k^2 r_0^2 / c_\nu^2)^{1+\nu}} - \frac{r_{core}^{2\nu}}{(1 + k^2 r_{core}^2 / c_\nu^2)^{1+\nu}} \right] \quad (19)$$

(3) *Triaxial Galaxies.* These profiles can be generalized to triaxial galaxies by introducing a change of variables to a new set of coordinates, $\vec{r} = \mathbf{F}\vec{u}$ and $\vec{q} = \mathbf{F}^{-1}\vec{s}$, so that we can rewrite our profiles,

$$g(\vec{r}) = \int d^n q \tilde{g}(\vec{q}) \exp(i\vec{q} \cdot \vec{r}), \quad (20)$$

in a new set of coordinates:

$$g(\mathbf{F}\vec{u}) = \det |\mathbf{F}^{-1}| \int d^n s \tilde{g}(\mathbf{F}^{-1}\vec{s}) \exp(i\vec{u} \cdot \vec{s}) \quad (21)$$

Applying the transformation, $k_x \rightarrow k_x \sqrt{1 - \epsilon}$ and $k_y \rightarrow k_y \sqrt{1 + \epsilon}$ the two dimensional light distribution in Fourier space becomes,

$$\Sigma_\nu(\vec{k}) = \frac{L_0}{\left[1 + k^2 \left(\frac{r_0}{c_\nu} \right)^2 (1 - \epsilon \cos(2\phi_k)) \right]^{1+\nu}} \quad (22)$$

which has a corresponding real space representation:

$$\Sigma_\nu(\vec{R}) = \frac{L_0 c_\nu^2}{r_0^2} f_\nu \left[\frac{c_\nu r}{r_0 \sqrt{1 - \epsilon^2}} \sqrt{1 + \epsilon \cos(2\phi_r)} \right] \quad (23)$$

We can expand out the Fourier space profile in a Taylor Series:

$$\Sigma_\nu(\vec{k}) = L_0 \sum_j \frac{\Gamma(2 + \nu)}{\Gamma(2 + \nu - j)j!} \frac{\left[\epsilon k^2 \left(\frac{r_0}{c_\nu} \right)^2 \cos(2\phi_k) \right]^j}{\left(1 + k^2 \left(\frac{r_0}{c_\nu} \right)^2 \right)^{1+\nu+j}} \quad (24)$$

3. The Effect of Seeing and Finite Resolution

In this section, we use the profiles to explore the effects of atmospheric seeing and telescope distortions on determinations of ellipticity.

The observed image, $I(\vec{r})$, is a convolution of the galaxy's surface brightness profile, $\Sigma(\vec{r})$ with the effects of the atmosphere and the telescope optics:

$$I(\vec{r}) = \int d^2k \exp(i\vec{k} \cdot \vec{r}) \Sigma(\vec{k}) R_{turb}(\vec{k}) R_{telescope}(\vec{k}) \quad (25)$$

where R_{turb} is the effect of atmospheric turbulence and $R_{telescope}$ is the response function of the telescope. Using Kolmogorov turbulence theory,

$$R(k) = \exp(-(kb)^{5/3}) \quad (26)$$

where $\theta_{FWHM} = 2.9207b$ and b is a parameter that characterizes the correlation length of the atmospheric turbulence. Since most astronomical observations are seeing-limited, we set $R_{telescope} = 1$ for this section.

Seeing reduces the signal/noise of the fits of galaxy (and star) profiles to the observations. We can estimate the signal to noise by considering fitting a multi-parameter model to the data:

$$\chi^2 = \sum_i \frac{\Delta\Omega}{n_0^2} [I_{measured}(r_i) - I_{model}(\vec{A}, r_i)]^2 \quad (27)$$

where n_0 is the noise times unit area, $\Delta\Omega$ is the area of the pixel, r_i is the pixel centroid, and $I_{measured}$ is the measured light profile and I_{model} is a model with a number of parameters

\vec{A} . The noise estimate assumes that we are observing faint galaxies and are dominated by atmospheric noise (and/or read noise).

The simplest case is a point source of intensity A :

$$\chi^2 = \sum_i \frac{\Delta\Omega}{n_0^2} [I_{measured}(r_i) - AI_{PS}(r_i)]^2 \quad (28)$$

. The signal-to-noise for point source detection is:

$$\left(\frac{S}{N}\right)_{PS}^2 = \frac{\partial\chi^2}{\partial A^2} = \sum_i \frac{I_{PS}^2(r_i)\Delta\Omega}{n_0^2} \quad (29)$$

In the continuum limit, we can use Parseval’s theorem to evaluate the signal-to-noise:

$$\begin{aligned} \left(\frac{S}{N}\right)_{PS}^2 &= \frac{1}{n_0^2} \int d^2r I_{PS}^2(r) \\ &= \frac{1}{n_0^2} \int d^2k R_a^2(\vec{k}) \equiv \frac{P_{PS}}{n_0^2} \end{aligned} \quad (30)$$

For a circularly symmetric galaxy fit with the profile of section 2, the observed profile can again be calculated by the convolution integral:

$$\begin{aligned} I_\nu^{(0)}(r) &= \int \frac{d^2k \exp[-i\vec{k} \cdot \vec{r}] \exp(-(kb)^{5/3})}{\left(1 + k^2 \left(\frac{r_0}{c_\nu}\right)^2\right)^{1+\nu}} \\ &= \frac{c_\nu^2}{r_0^2} \int \frac{\tilde{k} d\tilde{k} J_0(\tilde{k}r) \exp\left[-\left(\frac{\tilde{k}bc_\nu}{r_0}\right)^{5/3}\right]}{\left(1 + \tilde{k}^2\right)^{1+\nu}} \end{aligned} \quad (31)$$

where $\tilde{k} = kr_0/c_\nu$. The effect of atmospheric seeing is a function of b/r_0 or equivalently a function of the ratio of the FWHM of the PSF to the effective radius of the galaxy. Figures 4 and 5 show that atmospheric seeing “moves” light from the central cusp outwards and circularizes the inner portions of the galaxy. These effects are less dramatic for the outer isophotes.

The signal-to-noise for the galaxy detection is the second derivative of χ^2 with respect to M :

$$\left(\frac{S}{N}\right)_M^2 = \left(\frac{S}{N}\right)_{PS}^2 \frac{P_0}{P_{PS}} \quad (32)$$

where $(S/N)_{PS}$ is the signal-to-noise for the detection of a point source of the same magnitude.

$$P_0 = \int \frac{d^2\tilde{k}}{(1 + \tilde{k}^2)^{2+2\nu}} \exp \left[-2 \left(\frac{\tilde{k} b c_\nu}{r_0} \right)^{5/3} \right] \quad (33)$$

Note that the effect of galaxy finite size is to degrade the S/N by the ratio of the effective areas of a seeing convolved point source to the seeing convolved galaxy.

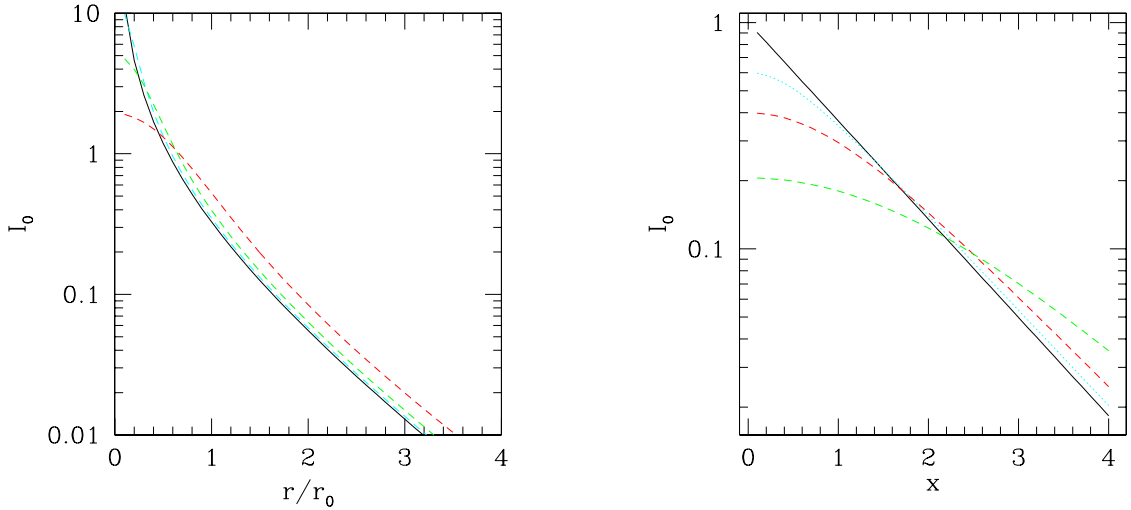


Fig. 4.— This shows the effects of seeing on the galaxy profile. The four lines in the left panel show the amplitude of the monopole term (Eq. 31) for $\theta_{FWHM}/r_0 = 0, 0.5, 1.0$ and 2.0 . The left panel is for an elliptical profile ($\nu = -0.6$) and the right panel is for an exponential profile ($\nu = 0.5$).

Seeing has an even more dramatic effect on the ellipticity of the image. The convolution of the $\cos(2\phi)$ term in the light profile,

$$\begin{aligned}
 I_\nu^{(1)}(r) &\equiv (1 + \nu) \left(\frac{r_0}{c_\nu} \right)^2 \int \frac{d^2k \exp \left[i\vec{k} \cdot \vec{r} \right] \exp \left(-(kb)^{5/3} k^2 \cos(2\phi_k) \right)}{\left(1 + k^2 \left(\frac{r_0}{c_\nu} \right)^2 \right)^{2+\nu}} \\
 &= \frac{\epsilon L_0 (1 + \nu) c_\nu^2}{r_0^2} \cos(2\phi_r) \int \frac{\tilde{k}^3 d\tilde{k} J_2(\tilde{k}r) \exp \left[- \left(\frac{\tilde{k} b c_\nu}{r_0} \right)^{5/3} \right]}{\left(1 + \tilde{k}^2 \right)^{2+\nu}}
 \end{aligned} \tag{34}$$

is shown in Figure 5. Seeing makes the central region of the galaxy round and has a reduced effect in the outer profile. Because the outer profile is less effected by seeing, it is useful to use a functional form that is a good fit to the outer profile for measurements of ellipticity. Galaxies are not well-described by Gaussians and the Hermite profile based determination of ellipticities are ”missing” the information in the outer profiles.

We can again estimate the signal to noise by differentiating the fit:

$$\chi^2 = \sum_i \frac{1}{\sigma_i^2} [I(r_i) - L_0 I_\nu^0(r_i) - \epsilon L_0 I_\nu^1(r_i)]^2 \tag{35}$$

Because the $\cos(2\phi)$ term is orthogonal to the symmetric term, the error on the second term is again just the second derivative with respect to its amplitude:

$$\sigma_{\epsilon L}^{-2} = \frac{1}{2} \left(\frac{S}{N} \right)_{PS}^2 \frac{\int r dr \left[I_\nu^{(1)}(r) \right]^2}{\int r dr \left[I_\nu^{(0)}(r) \right]^2} \frac{\int r dr I_\nu^{(0)}(r)}{\int r dr I_n u^{(1)}(r)} \tag{36}$$

where the (1/2) factor comes from angle averaging $\cos(2\phi_r)$. Using Parseval’s theorem and Equations (31- 34):

$$\sigma_{\epsilon L}^{-2} = \left(\frac{S}{N} \right)_{PS}^2 \frac{P_2}{P_0} \tag{37}$$

where,

$$P_2 = \frac{1 + \nu}{2} \left(\frac{c_\nu}{r_0} \right)^6 \int \frac{\tilde{k}^5 d\tilde{k}}{\left(1 + \tilde{k}^2 \right)^{4+2\nu}} \exp \left[-2 \left(\frac{\tilde{k} b c_\nu}{r_0} \right)^{5/3} \right] \tag{38}$$

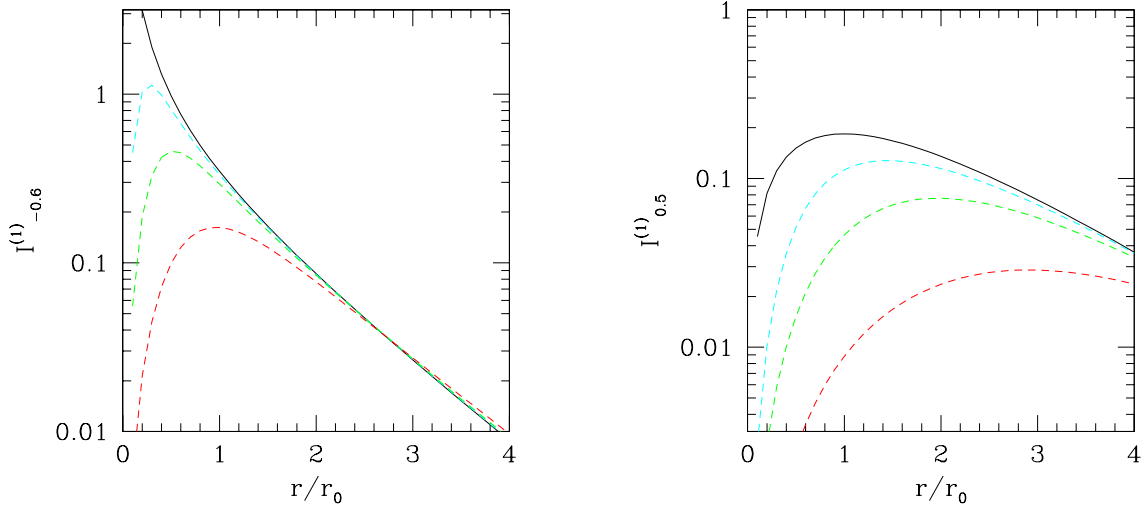


Fig. 5.— This shows the effects of seeing on the galaxy profile. The four lines in the left panel show the amplitude of the quadrupole term (Eq. 34) for $\theta_{FWHM}/r_0 = 0, 0.5, 1.0$ and 2.0 . The left panel is for an elliptical profile ($\nu = -0.6$) and the right panel is for an exponential profile ($\nu = 0.5$)

This yields:

$$\sigma_\epsilon^{-2} = \left(\frac{S}{N}\right)_{PS}^2 \frac{P_2 P_0}{(P_2 + P_0) P_{PS}} \quad (39)$$

Figure (6) quantifies the additional integration time needed to measure the ellipticity with an uncertainty, $\sigma_\epsilon = 1/5$ by plotting the point source signal to noise needed as a function of the ratio of the PSF FWHM to the effective radius of the galaxy,

$$\left(\frac{S}{N}\right)_{PS} = 5 \sqrt{\frac{(P_2 + P_0) P_{PS}}{P_2 P_0}} \quad (40)$$

Figure (4 - 6) show the effects of atmospheric seeing on lensing measurements. The left panels in Figures (4) and (5) show that as the seeing degrades, the image gets broader. While the right panel shows that as the seeing degrades, the images appear rounder, particularly in the inner regions. Note that seeing has less of an effect on the outer isophotes. Thus, high S/N observations can recover accurate ellipticity measurements, even if $\theta_{FWHM} > r_0$. However, since the information about the ellipticity is only in the outer isophotes, it is important to use an optimized weighting scheme.

4. Fitting the Profile to Observations

This section presents an algorithm for fitting light profiles to multi-image stacked data. The algorithm utilizes a linearized version of the two component light profile introduced in the previous section (see equation (42)). Since the goal of this approach is to have a fast linear algorithm that can be applied to large data sets, the profile is expanded in a power series in the image size and shape and the convolution of the seeing with each of the terms in the series is precomputed. Since we are also expanding the PSF in a series of terms, we can simultaneously fit for multi-frame images with little increase in computational cost. The final step in the fit is a non-linear step that is not very computationally intensive and returns the intensity, size, shape, profile, and orientation of each galaxy image.

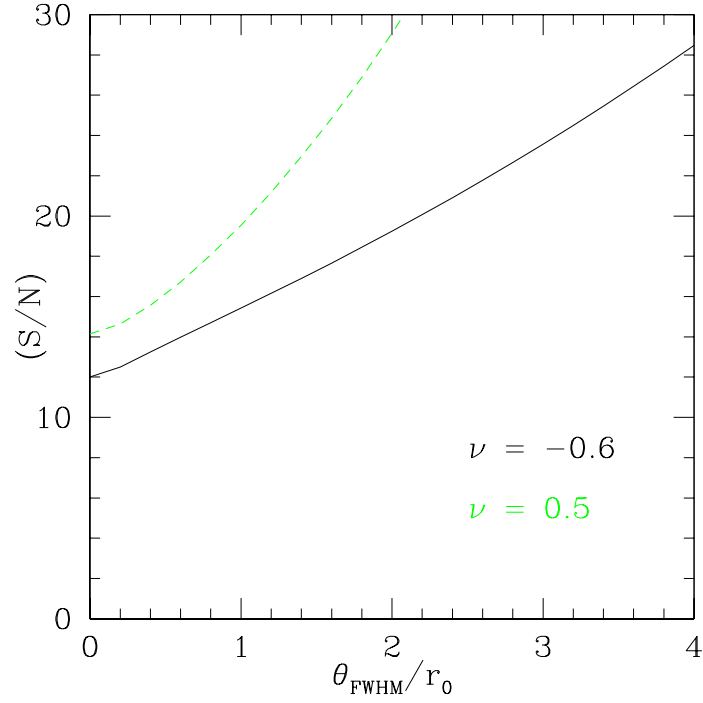


Fig. 6.— As the seeing degrades, longer integrations are needed to achieve the required sensitivity to shear. This figure quantifies this effect by plotting the point source S/N need to achieve a statistical error on the shearr of $\sigma_{e_j} = 0.2$. This point source S/N is shown as a function of the ratio of the FWHM of the PSF to the effective radius of the galaxy. The solid line is for a $\nu = -0.6$ profile, which corresponds to an elliptical galaxy. The dashed line is for a $\nu = 0.5$ profile, which corresponds to an exponential profile.

Following the approach outlined in section 2, the galaxy profile is parameterized as a five parameter fit: the amplitude of the exponential profile, L_1 , the amplitude of the elliptical M87-like profile term, L_2 , a flattening term, ϵ , a scale radius r_0 and an orientation, ϕ_0 :

$$\begin{aligned}\Sigma(\vec{r}|L_1, L_2, r_0, \epsilon, \phi_0) &= \Sigma_1(\vec{r}|L_1, r_0, \epsilon, \phi_0) + \Sigma_2(\vec{r}|L_2, r_0, \epsilon, \phi_0) \\ &= L_1\alpha_1 f_{1/2} \left(c_{1/2} \frac{r\sqrt{1 + \epsilon \cos(2(\phi - \phi_0))}}{r_0} \right) \\ &\quad + L_2\alpha_2 f_{-0.85} \left(0.35 \frac{r\sqrt{1 + \epsilon \cos(2(\phi - \phi_0))}}{r_0} \right)\end{aligned}\tag{41}$$

where $\alpha_1 = \exp(1.6783) = 1/f_{1/2}(c_{1/2})$ and $\alpha_2 = 1/f_{-0.85}(0.35)$. This fit has a simple representation in Fourier space:

$$\sum_{i=1,2} \frac{L_i}{\{1 + k^2\gamma_i^2 r_0^2 [1 - \epsilon \cos(2(\phi - \phi_0))]\}^{1+\nu_i}}\tag{42}$$

where $\nu_1 = 0.5$, $\nu_2 = -0.85$, $\gamma_1 = 1/c_{1/2}$, and $\gamma_2 = 1/0.35$. Note that we are fitting a single value of r_0 , the effective radius to the profile.

The first step in the analysis is to fit for the position of the galaxy, $\vec{\theta}_g$ and estimate its size from measuring its half light radius. By first computing the convolution of a series of circularly symmetric galaxy profiles with different characteristic size (e.g., in steps of 0.1"), the profile fitting calculation becomes a linear problem. Instead of fitting for r_0 , the effective radius, we can fit for

$$\Delta \equiv 1 - \left(\frac{r_0}{r_i} \right)^2\tag{43}$$

where r_i is one of the nearest precomputed fit to the initial list of values . Expanding the profile as a Taylor series in $(\Delta + (1 - \Delta)\epsilon \cos(2(\phi - \phi_0)))$:

$$\begin{aligned}\Sigma(\vec{k}|L_1, L_2, \Delta, \epsilon, \phi_0) &= \sum_i \frac{L_i}{[1 + k^2\gamma_i^2 r_0^2 (1 - \Delta)(1 - \epsilon \cos(2(\phi - \phi_0)))]^{1+\nu_i}} \\ &= \sum_i \sum_{j=0} [\Delta + (1 - \Delta)\epsilon \cos(2(\phi - \phi_0))]^j \frac{w_j(\nu_i)(\gamma_i k r_0)^{2j}}{[1 + \gamma_i^2 k^2 r_0^2]^{\nu_i+j+1}}\end{aligned}\tag{44}$$

where $w_j(\nu_i) = \prod_{s=1}^j (\nu_i + s)/j!$. We then rewrite the profile as a sum of terms with linear fit coefficients:

$$\Sigma_i(\vec{k}|a_q) = \sum_{jm} a_{ijm}(L_1, L_2, \Delta, \epsilon, \phi_0) \mu_{ijm}(\vec{k}, r_i) = \sum_q a_q \mu_q(\vec{k}, r_i) \quad (45)$$

where the sum over i, j and m is represented as a sum over q for notational simplicity:

$$a_{ijm} = L_i \Delta^{j-m} (1 - \Delta)^m \epsilon^m \exp(-2im\phi_0), \quad (46)$$

and

$$\mu_{ijm}(\vec{k}, r_i) = \frac{j!}{(j-m)!m!} \frac{(\gamma_i k r_i)^{2j} w_j(\nu_i) \exp(2im\phi)}{[1 + \gamma_i^2 k^2 r_i^2]^{\nu_i+j+1}}. \quad (47)$$

The next step is to represent the time-varying and spatially varying PSF can be expanded as a sum of specified (but not necessarily orthogonal functions), P_s (see e.g., (Jarvis & Jain 2004)):

$$R_{PSF}(\vec{k}, \vec{\theta}_g, t_n) = \sum_s U_s(\vec{\theta}_g, t_n) P_s(\vec{k}), \quad (48)$$

] where t_n is the time of each frame, θ_g is the galaxy position, and $P_s(\vec{k})$ is the Fourier transform of the basis function. Typically, $U_s(\vec{\theta}_g, t_p)$ will be fit to stars in the image.

The image profile in a given frame can now be expressed as a sum,:

$$\tilde{I}(\vec{r}, t_n | \vec{a}_q) = \sum_q a_q \sum_s U_s(\vec{\theta}_g, t_n) \tilde{\mu}_{qs}(\vec{r}, r_i), \quad (49)$$

over a series of terms that can be precomputed once for a series of effective radii, r_i :

$$\tilde{\mu}_{qs}(\vec{r}) = \int d^2k \exp(-i\vec{k} \cdot \vec{r}) P_s(\vec{k}) \mu_q(\vec{k}, r_i) \quad (50)$$

These function, $\tilde{\mu}_{ijms}$, describe the convolution of a term in the expansion of the galaxy light profile with a term in the expansion of the PSF.

Fitting the convolved linear profile to the observations is now a linear process that fits the galaxy light profile coefficients, a_k , to all of the data in the stack:

$$\chi^2 = \sum_{l,n} \frac{(I_{\text{measured}}(\vec{r}_l, t_n) - \sum_q a_q \sum_s U_s(\vec{r}_g, t_n) \tilde{\mu}_{qs}(\vec{r}, r_i))^2}{\sigma_{ln}^2} \quad (51)$$

where the sum over l is a sum over pixels. The best fit is the solution to a linear equation,

$$N_{qq'}^{-1} a_{q'}^{ML} = b_q \quad (52)$$

where

$$N_{qq'} = \sum_{ln} \frac{\tilde{\mu}_q(\vec{r}_l, t_n) \tilde{\mu}_{q'}(\vec{r}_l, t_n)}{\sigma_{ln}^2} \quad (53)$$

$$b_q = \sum_{ln} \frac{I_{measured}(\vec{r}_l, t_n) \tilde{\mu}_q(|vecr_l, t_n)}{\sigma_{ln}^2} \quad (54)$$

are evaluated as a sum over pixels and frames using precomputed functions. This linear fit takes $N_{stack} N_{pix} N_{galterms}^2$ steps to evaluate N_{kk} and $N_{galterms}^3$ steps to invert the matrix. If we expand to first order in the ellipticity, then $N_{galterms} = 6$. If we work to fourth order, then $N_{galterms} = 15$. This very rapid process should enable fits to individual observations in the stack.

We then do a nonlinear fit to solve for the amplitude of the terms in the expansion, L_1 , L_2 , ϵ , ϕ_0 , and Δ :

$$\chi^2(a_q | L_1, L_2, \Delta, \epsilon, \phi_0) = \sum_{qq'} [a_q^{ML} - a_q^{fit}(L_1, L_2, \Delta, \epsilon, \phi_0)] N_{qq'}^{-1} [a_{q'}^{ML} - a_{q'}^{fit}(L_1, L_2, \Delta, \epsilon, \phi_0)] \quad (55)$$

where a_q is defined in Equation (46). This operation is very quick as it takes only $5N_{galterms}$ steps to evaluate the non-linear fit.

5. Conclusions and Next Steps

This note introduces a basis function that may prove useful for the analysis of galaxy images, particularly for lensing work. In a subsequent paper, we will test this approach against the GREAT08 simulations (Bridle et al. 2009).

There are several possible extensions to this parameter fit. We can include priors on ϵ and modified the χ^2 (Equation (55)) to be a likelihood function and then marginalize over the galaxy size and position. We could then also include priors on the ellipticity functions (Kitching et al. 2008). Other possible generalization would be to include PSF uncertainties and to generalize the expansion to include shapelet terms.

6. Acknowledgements

This research was partially supported by NSF grant AST/0908292 through the ARAA. I would like to thank Alan Heavens, Chiaki Hikage, Robert Lupton, Rachel Mandelbaum, Michael Strauss and Masahiro Takada for helpful comments.

REFERENCES

- Abramowitz, M., & Stegun, I. A. 1972, Handbook of Mathematical Functions
- Bernstein, G. M., & Jarvis, M. 2002, *Astron. J.*, 123, 583
- Bridle, S., et al. 2009, ArXiv e-prints
- Hoekstra, H., & Jain, B. 2008, Annual Review of Nuclear and Particle Science, 58, 99
- Jarvis, M., & Jain, B. 2004, ArXiv Astrophysics e-prints
- Kitching, T. D., Miller, L., Heymans, C. E., van Waerbeke, L., & Heavens, A. F. 2008, *Mon. Not. Royal Astron. Soc.*, 390, 149
- Kormendy, J., Fisher, D. B., Cornell, M. E., & Bender, R. 2009, *Ap.J. (Supp.)*, 182, 216
- Kostroun, V. 1980, Nuclear Instruments and Methods, 172, 371
- Ngan, W., van Waerbeke, L., Mahdavi, A., Heymans, C., & Hoekstra, H. 2009, *Mon. Not. Royal Astron. Soc.*, 396, 1211

A. Appendix: Useful Properties of Bessel Functions and Incomplete Bessel Functions of the Third Kind

Kostroun (1980) provides a useful expression for the numerical evaluation of $K_\nu(u)$:

$$K_\nu(u) = h \left[\frac{\exp(-u)}{2} + \sum_{r=1}^{\infty} \exp(-u \cosh(rh)) \cosh(\nu rh) \right] \quad (\text{A1})$$

where for values of ν of interest to this paper, we set $h = 0.5$ and find that the sum converges to 10^{-10} with less than 7 terms for most values of ν and u used in the paper.

There are useful relationships between various modified Bessel functions:

$$\int J_m(kr) \frac{k^{m+1} dk}{(1+k^2)^{1+m+\nu}} = \left(\frac{r}{2}\right)^{m+\nu} \frac{K_\nu(r)}{\Gamma(1+m+\nu)} \quad (\text{A2})$$

$$\begin{aligned} \int j_m(kr) \frac{k^{m+2} dk}{(1+k^2)^{1+m+\nu}} &= \left(\frac{r}{2}\right)^{m+\nu-1/2} \frac{\sqrt{\pi} K_{\nu-1/2}(r)}{\Gamma(1+m+\nu)} \\ &= \left(\frac{r}{2}\right)^m f_{\nu-1/2}(r) \frac{\sqrt{\pi} \Gamma(\nu+3/2)}{\Gamma(1+m+\nu)} \end{aligned} \quad (\text{A3})$$

For $\nu < 0$, we can use Abramowitz & Stegun (1972) equation 9.6.25,

$$\begin{aligned} f_\nu(z) &= \frac{\sqrt{\pi}}{\Gamma(\nu+1)\Gamma(\nu+1/2)} \int_0^\infty \exp(-z \cosh t) \sinh^{2\nu} t dt \\ &= \frac{\sqrt{\pi}}{\Gamma(\nu+1)\Gamma(\nu+1/2)} \int_1^\infty \frac{\exp(-zu)}{(u^2-1)^{1/2-\nu}} du \end{aligned} \quad (\text{A4})$$

Thus,

$$\int_x^\infty f_\nu(z) dz = \frac{\sqrt{\pi} \exp(-x)}{\Gamma(\nu+1)\Gamma(\nu+1/2)} \int_0^\infty \frac{\exp(-xv)}{(1+v)(v(2+v))^{1/2-\nu}} dv \quad (\text{A5})$$

Expanding $1/(1+v)/(2+v)^{1/2-\nu}$ in a Taylor series and integrating yields:

$$\int_x^\infty f_\nu(z) dz = \frac{\sqrt{\pi} \exp(-x)}{2^{\nu-1/2} \Gamma(\nu+1)\Gamma(\nu+1/2)} \sum \frac{(-1)^j \Gamma(\nu + \frac{1}{2} + j)}{(x)^{1/2-\nu-j}} \left[1 + \frac{w_j(1/2-\nu)}{2^j j!} \right] \quad (\text{A6})$$

where $w_0(\mu) = 0$, $w_1(\mu) = \mu$, $w_2(\mu) = 5\mu + \mu^2$, $w_3(\mu) = 32\mu + 9\mu^2 + \mu^3$, and $w_4(\mu) = 262\mu + 83\mu^2 + 14\mu^3 + \mu^4$. Using Abramowitz & Stegun (1972) equation 9.6.28,

$$\left(\frac{1}{z} \frac{d}{dz}\right)^m f_\nu(z) = \left(\frac{-1}{2}\right)^m \frac{\Gamma(\nu-m+1)}{\Gamma(\nu+1)} f_{\nu-m}(z) \quad (\text{A7})$$